
Reproducible measures of correlative and causal brain connectivity

 **Cooper J. Mellema**^{1,2,5}

 **Albert Montillo, PhD**^{1,2,3,4,5}

¹Lyda Hill Department of Bioinformatics

²Biomedical Engineering Department

³Advanced Imaging Research Center

⁴Radiology Department

⁵University of Texas Southwestern Medical Center

Cooper.Mellema@UTSouthwestern.edu

Albert.Montillo@UTSouthwestern.edu

Abstract

Patterns of interregional brain connectivity characterize the function of the human nervous system in both health and disease. Such connectivity can be inferred non-invasively by analyzing the blood-oxygen-level-dependent (BOLD) signal from functional magnetic resonance imaging (fMRI). However, approaches to quantify this connectivity must solve an under-constrained problem with several potential solutions due to noise and spatial resolution limitations during imaging. Previous research has insufficiently evaluated the reproducibility of the traditional approaches and these approaches have been insufficiently regularized to increase solution stability. We propose three new measures of correlative and causal connectivity which incorporate explicit regularization through a structural connectivity prior from diffusion MRI. These new measures, which exploit a machine learning formulation for efficient computation, are evaluated against traditional measures for reproducibility and predictive power. In particular, correlation, partial correlation, spectral density, and a novel measure of functional connectivity based on machine learning feature importance are compared. Additionally, measures of effective connectivity are compared to two proposed connectivity measures: a machine learning approach and a Granger-causal approach incorporating a low-dimensional projection with a diffusion MRI-derived tractography prior. In addition to reproducibility, we quantify the capacity each measures has to infer three study participant traits: a physiologic trait, a cognitive trait, and a combined physiologic and cognitive trait. Of these methods, the proposed machine learning based functional connectivity method and the traditional partial correlation approaches achieve high reproducibility and accuracy predicting the traits, while the proposed machine-learning based causal connectivity measure achieves the highest reproducibility and predictive accuracy. Attaining both high reproducibility and predictiveness across a variety of neurobiological targets demonstrates the strong potential for the proposed connectivity measures to be broadly used in future neuroimaging studies.

Keywords fMRI, connectivity, functional connectivity, effective connectivity, reproducibility, patterns

1 Introduction

It is generally believed that the connectivity of the human brain is integral to cognitive capacity, can be an early marker for human disease, and underlies the fundamental functioning of the central nervous system. However, measuring that connectivity in living people has proven problematic [1–3]. Functional magnetic resonance imaging (fMRI) measures the blood-oxygen-level-dependent (BOLD) signal, a surrogate for neural activity. Using an atlas, the brain scan can be parcellated into brain regions and the mean regional time series can be computed from the fMRI voxels in each region. By measuring temporal relationships between the mean BOLD signal from two or more regions of the brain, the underlying direct and indirect

connectivity and communication within the brain can be probed. The connections between regions can then be used to represent the participant specific connectome as a connectivity graph with each region represented as a node in the graph and edges between nodes with edge strength proportion to the pairwise regional connectivity.

Connectivity metrics can be grouped into undirected functional connectivity (FC) metrics and directed effective connectivity (EC) metrics. These measures are calculated from fMRI with a measure of similarity or information transfer between mean regional BOLD timeseries. Each BOLD timeseries is a surrogate for underlying neural activity, thus EC and FC capture relationships between regional activity in fMRI. *Functional connectivity* is defined as the temporal coincidence of spatially distant neurophysiological events [4] and it has been used successfully to characterize the human connectome in both health and disease [5, 6]. This is traditionally calculated with correlation or partial correlation. Meanwhile, *effective connectivity* is defined as the influence one neural system exerts over another [4]. Broadly, this is a model-dependent measure wherein the information transfer between mean regional timeseries is quantified from the goodness of fit of a model that predicts one of the timeseries from one or more of the other timeseries. Examples of EC measures include Granger causality [7–10], dynamic causal modeling [11, 12], and structured equation modeling [1], which all have been widely deployed for connectome characterization. EC is inherently directional as it captures the direction of information flow over time [13]. EC is model-dependent and requires more computation than FC but suppresses spurious indirect connections and identifies linkages that are potentially causal and not simply correlated.

Traditional FC and EC measures have several limitations, for which we propose potential solutions. Common FC measures include Pearson’s r , partial correlation, and instantaneous spectral density (also called “spectral Granger causality”, which is not a true EC measure because it does not use the past history of the independent timeseries) [14]. Each of these methods measure a degree of linear association between two mean regional timeseries. However, the actual relationship between mean regional brain activity is not linear [12]. Therefore, our first set of innovations use nonlinear machine learning models to better capture such nonlinearities when measuring functional connectivity. Of the different EC measures, we have focused on Granger causal (GC) methods as they are a data-driven approach that can handle a large number of regions in the model. Modern fMRI connectivity analysis typically uses hundreds of regions, which dynamic causal modeling and structured equation modeling cannot handle as they apply an exhaustive search of possible patterns of connectivity. For these latter methods, the number of models fitted scales as $O(N!)$ where N is the number of regions. They may alternatively use a prior to constrain the potential solution space, which may not be available for a given use case and thus may miss interactions of importance [1, 12]. There are several limitations to Granger causality such as model selection procedures, regularization, scaling (classical GC scales with $O(N^2)$ models fitted), capturing nonlinear interactions, and incorporating prior information [4]. However, we propose two new measures of effective connectivity which address these issues. First, we propose using learned features from a nonlinear machine learning model to better capture nonlinearities in the timeseries relations, whose number of required models to be fitted scales as $O(N)$, and addresses model selection and regularization by ensembling simpler predictive models. Our second proposed improvement is to regularize using a structural connectivity prior derived from diffusion MRI. We perform streamline tractography from diffusion MRI and use the number of streamlines connecting regions as a quantitative measure of structural connectivity. We constrain interactions between regional timeseries to prefer to lie along putative fiber bundles. Actual neural communication occurs through such physical connections, so this constraint is a natural choice of a prior to guide brain functional connectivity [15–19]. We also project the mean regional timeseries into a low dimensional space informed by the streamline structural connectivity prior before following a GC approach in this low dimensional space. Performing the GC calculation in a low dimensional space affords several

advantages including: simplification of model selection as there are fewer parameters to tune, regularization in the calculation, and incorporated prior information from diffusion MRI. Each of our proposed approaches is evaluated for reliability and the ability to predictive cognitive and physiological traits of the participants in our study.

To evaluate the proposed FC and EC measures, we examined each measure’s reproducibility across four repeated fMRI scans of the each individual in our Human Connectome Project (HCP)-derived dataset. A connectivity measure should produce a similar connectivity matrix for a given individual across such repeat fMRI scans that are acquired within a short window of time. A measure that is reproducible better captures an individual’s underlying connectivity fingerprint and is therefore more useful to characterize differences between individuals [20, 21]. In addition to reproducibility, there is growing interest to use connectivity for a variety of predictive tasks. Some of these potential targets include fluid intelligence, vascular health, and the individual subject stress level [21–24]. Therefore, we also measure the predictive power of each FC and EC metric in three relevant domains: a purely physiological domain predicting mean arterial pressure, a purely cognitive domain measuring fluid intelligence, and a combined physiologic and cognitive domain measuring stress. These were chosen as a representative subset of targets of interest to researchers and/or clinicians as they could assist predictions for physiology (e.g., stroke, aging), cognition (e.g., memory, PTSD), or a combination of the two (e.g., stress, neurodegeneration) for better diagnoses and treatment. Measures that are both reproducible and have consistently high predictive power across multiple tasks are significantly more useful as candidate biomarkers. These improved biomarkers will help advance the study of human brain connectivity in health and disease.

2 Methods

2.1.1 Proposed machine learning-based functional connectivity (MLFC) measures

Characterizing brain connectivity to better understand both health and disease is a complex process. We propose measuring associations between regions to include both linear and nonlinear aspects of information transfer. Central to this premise, we propose the construction of a machine learning model to calculate functional connectivity, an approach we will denote MLFC. This model predicts the activity at a given node j by using the information present at all other nodes (brain regions) at any given time t . As illustrated in **Equation 1**, we use a nonlinear model M to predict the activity at region j from all other regions $i \notin j$.

$$\langle a \rangle_{j,t} = M(\langle a \rangle_{i \notin j,t}), \quad a = \text{activity} \quad (1)$$

This model can, if chosen appropriately, simultaneously capture the association between all other nodes’ activity and the target node j . The weight (or other measure of feature importance) assigned to each covariate *quantifies* the amount of information the model is using from that node to predict the target node j , which is a putative measure of the *connectivity* between each node i and j . This draws partly on theory from Granger Causality literature, which has used the coefficients of a bilinear model to quantify instantaneous information transfer (i.e. the relationship between signals at a fixed single time t) by predicting the activity of node j at time t from other nodes i with a linear model [14, 25].

In resting state fMRI, we want to derive a measure of functional connectivity between every set of nodes, resulting in a functional connectivity (FC) matrix. The above described procedure using the weight or feature importance of a predictive model fills one row of the matrix at a time. If we repeat the process for each region, we fill the entire FC matrix by fitting N models, meaning this procedure scales as $O(N)$.

The choice of model M determines what associations we can detect between regions from the predicted covariate weights. Previous work has used an extremely random trees model [26]. However, this work did not compare to other machine learning models, did not quantify reproducibility of the approach, and did not extend the approach to the more theoretically rich directed information transfer which includes time delays. We use multiple additional models, quantify both reproducibility and predictive power across several relevant target domains, and we extend the approach to time-directed influence with our machine-learning effective connectivity (MLEC) approach.

To overcome the modeling limitations, we not only use the ERT transfer model M but also extend the approach with nonlinear radial basis function kernel SVM and XGBoost models. The SVM is a high-performing machine learning model which is both regularized differently has a more directly interpretable weight than the ERT, as each coefficient has an explicit covariate weight in the model. The XGBoost approach tends to have higher performance than the ERT, and importantly, has a more robust regularization to handle multicollinearity from repeated sub-sampling of the data, which we hypothesize will better handle correlated regions than the native ERT approach.

We follow the following procedure in our model fitting approach for each proposed model. First, the mean timeseries per region is standard-scaled to unit variance centered at 0. Then, a model is fit to predict regional activity at node j at every time t from other all other nodes i at each time t . Then, a measure of feature weight or importance is extracted from the model for each covariate i . We repeat this for each node j to fully populate an asymmetric FC matrix. The asymmetric matrix is then symmetrized by averaging itself with its transpose.

In addition to the above common approach, each model has some individual differences in the FC calculation. Firstly, the measure of feature importance or weight is calculated differently for each model. For the ERT model, we use the Gini importance as this feature importance weight. For the SVM, we use the covariate weight. And for the XGBoost model, we use the Gini importance weighted by the number of samples routed through any given decision node. Secondly, the determination of hyperparameters is specific for each model. A two-step approach is used to fit the XGBoost models. In the first step, a group-level model to predict each brain region’s activity from data pooled from all subjects is fit and hyperparameter optimized with a Bayesian Optimization HyperBand (BOHB) search of 2000 model configurations. This identifies reasonable values for a few general hyperparameters: the maximum depth, learning rate, L1 and L2 regularization, and minimum loss per split. For the second step, we fit a subject-specific model for EC calculation using the hyperparameters found in step 1. This is done by training the model with an equal weight on the target subject, as well as a regularization prior consisting of all other subjects (e.g. the Model must fit both the specific subject as well as the population of subjects, with an equal weighting on each). Tree-based models are not readily adapted for incremental learning, so rather than tuning a group-level model on subject specific data, we use a combined dataset as recommended by the XGBoost developers [27]. The ERT and SVM models did not benefit from a hyperparameter search relative to their default parameters, and the default parameters are used going forward.

In order to evaluate the relative benefits of each proposed MLFC measure, we test each FC measure’s reproducibility and evaluate its average predictive power by using it to infer 3 individual traits of interest (see **Section 2.4** for further information on the respective traits).

Algorithm 1: GC algorithm

Input: Regional time series $\mathbf{X}_t^i, (i \in [1, N], t \in [1, T])$ where N is the number of regions and T is the number of timepoints, max lag τ , timeseries predictor \mathbf{f} ; **Output:** Effective connectivity matrix \mathbf{E} ;

For the initial regional timeseries \mathbf{X} with N regions;

```
for  $i := 1$  to  $N$  do Full model
   $\mathbf{X}_t^i = \mathbf{f}(\mathbf{X}_{t-1}, \mathbf{X}_{t-2}, \dots, \mathbf{X}_{t-\tau})$  Fit a full model  $\mathbf{f}$  predicting activity  $\mathbf{X}$  at time  $t$  and node  $i$  from times  $t-1, \dots, t-\tau$ ;
  for  $j := 1$  to  $N$  do Reduced model
     $\mathbf{X}' = \mathbf{X}_{j \setminus N}$  drop column  $j$  from timeseries  $\mathbf{X}$ ;
     $\mathbf{X}_t^i = \mathbf{r}(\mathbf{X}'_{t-1}, \mathbf{X}'_{t-2}, \dots, \mathbf{X}'_{t-\tau})$  Fit a reduced model  $\mathbf{r}$  predicting activity  $\mathbf{X}'$  at region  $i$  at time  $t$  from times  $t-1, \dots, t-\tau$ ;
     $\mathbf{E}_{i,j} = \log(\sigma(\mathbf{f}_{error})/\sigma(\mathbf{r}_{error}))$  the EC score between  $i$  and  $j$  equals the log of the ratio of the standard deviation of the residuals of the full and reduced model;
  end
end
end
```

2.1.2 Background of effective connectivity

In addition the functional connectivity, brain connectivity can be quantified with measures of time-delayed information transfer, which we will call “effective connectivity” measures. Effective connectivity can be quantified in numerous ways: multivariate Granger-causal (GC) scores [9, 10, 28], bilinear Granger-causal modeling [25], and other measures of directed neural influence [13]. This paper builds primarily on principles of Granger causal modeling. Granger-causal measures define a directed edge by quantifying how the past history of signal B informs the future activity of signal A. In neuroimaging, region B is said to be Granger causal of A if a model to predict the future of A given all past information from all regions including B is more accurate than a model that doesn’t include B. The degree of causality is called the GC score [7]. We will build upon classical GC methodologies in two ways: by extending the traditional GC modeling with machine learning models, and by extending the traditional GC modeling with dimensionality reduction approaches.

Before outlining the approaches by which we extend GC, we will first walk through the standard GC methodology. To generate a Granger causal effective connectivity matrix, the Granger score between the average regional timecourses from each pair of regions is calculated using GC **Algorithm 1**. A full model f is fit to predict activity in region i at time t from the past history of all regions. Then, a reduced model f' is fit to predict the same activity at time t from the past history of all regions except j . The EC score becomes the log of the ratio of the standard deviation of the residuals of the full and reduced models. By using a linear model f , a baseline measure of effective connectivity can be calculated. The linear models with which we calculate the GC score include: an unpenalized multivariate autoregressive model, an elastic multivariate autoregressive model with a small L_1 and L_2 penalty ($L_1 = L_2 = \lambda = 0.1$), and an elastic multivariate autoregressive model with a large L_1 and L_2 penalty ($\lambda = 10$). These regularization amounts were chosen empirically to be representative of strong and weak regularization. The timeseries is tested for significant autoregression with the Augmented Dickey Fuller test and any significant autoregression is removed prior to model fitting. Lag values (autoregressive order) of 1-5 times repetition time (TR) were tested and the model using the lag with the lowest Akaike information criterion (AIC) was selected independently for each regional model. We denote the three models f which we compare (unpenalized linear, elastic with $\lambda=0.1$, and elastic with $\lambda=10$) GC , $Elastic_{\lambda=0.1}GC$ and $Elastic_{\lambda=10}GC$.

Algorithm 2: MLEC algorithm

Input: Regional time series $\mathbf{X}_t^i, (i \in [1, N], t \in [1, T])$ where N is the number of regions and T is the number of timepoints, max lag τ , timeseries predictor \mathbf{f} ; **Output:** Effective connectivity matrix \mathbf{E} ;

For an initial regional timeseries \mathbf{X} with N regions ;

for $i := 1$ **to** N **do** *Full model*

$\mathbf{X}_t^i = \mathbf{f}(\mathbf{X}_{t-1}, \mathbf{X}_{t-2}, \dots, \mathbf{X}_{t-\tau})$ Fit a machine learning model \mathbf{f} predicting activity \mathbf{X} at region i at time t from times $t-1, \dots, t-\tau$;

if $\mathbf{f} = \text{ERT or XGB Predictor}$ **then**

$G(\mathbf{f})_j = \sum_{n=1}^C P(p(n) * 1 - p(n))$ the Gini impurity, where p is the probability of the data being routed down a split, P is the proportion of data that was routed to that split, and C is the set of all nodes that use feature j ;

else if $\mathbf{f} = \text{SVM Predictor}$ **then**

$G(\mathbf{f}) = w$ given the SVM optimization;;

$\min ||w||^2 + C \sum (\eta_i)$ subject to $y_i(w \cdot \theta(x_i) + b) \geq 1 - \eta_i, \eta_i \geq 0$;

$\mathbf{E}_i = G(\mathbf{f})$, row i of EC matrix = feature importance of \mathbf{f} ;

end

2.1.3 Proposed machine learning-based effective connectivity (MLEC) measures

For our first proposed improvement on EC, we develop a novel EC approach using machine learning. We draw upon the classical GC approximation where, rather than fitting a full and reduced model f , as in **Algorithm 1**, we instead quantify the EC with the model coefficients [15, 25]. This is also closely related to the MLFC approach [26] described in **Section 2.1.1** above, but with a time-delay included. We calculate these metrics by using a machine learning model to predict future timesteps given past timesteps and identify the important learned features of that model, as detailed in **Algorithm 2**. Our proposed method improves upon GC by capturing directed influence with only one model fit per region tested, scaling as $O(N)$ rather than $O(N^2)$ where N is the number of regions, by avoiding the inner loop from **Algorithm 1**. Furthermore, the machine learning approaches capture nonlinear interactions which the standard GC approaches do not. We denote this Machine learning effective connectivity approach MLEC. We use both: an extremely random trees predictor and a support vector regressor with a radial basis function kernel. We do not use XGBoost as in the MLEC approach because the added lag drastically increases the likelihood of overfitting and makes the success of the hyperparameter optimization uncertain, potentially confounding results. The machine learning approach with the extremely random trees model we denote $MLEC_{ERT}$ and the machine learning approach with the support vector regressor $MLEC_{SVM}$.

2.1.4 Proposed structurally-projected effective connectivity (SPGC) measures

Our second proposed improvement upon GC constructs Granger causal models in a lower dimensional space informed by a prior from diffusion MRI to constrain EC along true pathways of communication [15–19]. We denote this Structurally Projected Granger Causality approach SPGC. The algorithm for this proposed approach is presented in **Algorithm 3**. This approach projects the timeseries down into a lower dimensional representation and calculates a full and reduced model in the low dimensional space before projecting the predicted activity back into real space and finding the error in full versus reduced models. Our proposed improvement encourages low dimensional timeseries components that are structurally likely by constraining the calculated components' low dimensional representation to lie along known structural networks. This approach also incorporates a sparsity constraint from sparse PCA. Sparse PCA minimizes the number of nonzero terms in each principal component while maximizing the variance explained by the components [29]. This sparsity prior and the prior from the structural connectivity matrix derived from diffusion MRI encourages these components to robustly represent a physically connected sub-network of the brain.

Algorithm 3: SPGC algorithm

Input: Regional time series $\mathbf{X}_t^i, (i \in [1, N], t \in [1, T])$ where N is the number of regions and T is the number of timepoints, transformation matrix Φ where Φ is either the coarse or fine projection from prior informed sparse PCA (Equation 1), max lag τ timeseries predictor \mathbf{f} ; **Output:** Effective connectivity matrix \mathbf{E} ;

For an initial regional timeseries \mathbf{X} with N regions ;

for $i := 1$ **to** N **do** *Full model*

$\theta = \mathbf{X} \cdot \Phi$, where Φ is the transformation matrix to the structurally constrained low dimensional space (Equation 1);

$\mathbf{X}_t^i = \mathbf{f}(\theta_{t-1}, \theta_{t-2}, \dots, \theta_{t-\tau}) \cdot \Phi^T$ Fit a model \mathbf{f} predicting activity \mathbf{X} at time t from times $t-1, \dots, t-\tau$;

for $j := 1$ **to** N **do** *Reduced model*

$\theta' = \mathbf{X} \cdot \Phi_{j \setminus N}$, where $\Phi_{j \setminus N}$ is the transformation matrix to the structurally constrained low dimensional space (Equation 1) with column j removed;

$\mathbf{X}_t^i = \mathbf{r}(\theta'_{t-1}, \theta'_{t-2}, \dots, \theta'_{t-\tau}) \cdot \Phi_{j \setminus N}^T$ Fit a model \mathbf{r} predicting activity \mathbf{X} at region i at time t from times $t-1, \dots, t-\tau$;

$\mathbf{E}_{i,j} = \log(\sigma(\mathbf{f}_{error}) / \sigma(\mathbf{r}_{error}))$ the EC score between i and j equals the log of the ratio of the standard deviation of the residuals of the full and reduced model;

end

end

The physical connectivity prior for the low-dimensional projection of the timeseries comes from a structural connectivity matrix from diffusion MRI. The structural connectivity matrix is calculated from an average tractogram from all 1065 subjects in the human connectome project (HCP) as computed in [30] and the number of streamlines passing through each region of interest. This results in a population-level prior, rather than an individually formatted prior. This constraint may be a more faithful representation of the underlying brain functionality as true connectivity lies sparsely along physical connections [15–19]. The meaning of ‘structural connectivity’ (SC) is complex. There are a plethora of both direct and indirect connections in the brain, and both direct and indirect connections are captured through the streamline-derived prior. Each streamline can represent multisynaptic or monosynaptic fibers. However, in formulating a prior from SC, we constrain activity to lie largely along the streamline populations. So, connections mediated mostly by intermediate nodes, such as an indirect connection from region A to region C through intermediate region B, are explicitly modeled rather than a connection from region A to C being inferred directly. While the concept of using structural connectivity from tractography to constrain fMRI interpretation has been used before [15, 16] to interpret fMRI, the combination with dimensionality reduction is novel to this work.

We use a formulation of prior-constrained sparse PCA to incorporate our SC prior in the timeseries dimensionality reduction. The objective function for this constrained sparse PCA shown in **Equation 2**; adapted from Dhillon et al. [31] to include the tractography prior:

$$\vec{v}_i^* = \underset{v_i, \|v_i\|=1, v_i^T \mathbf{P}_i = 0, v_j=0, i \neq j, v_i \geq 0}{\operatorname{argmax}} (\vec{v}_i^T (\mathbf{C} + \theta \cdot \mathbf{P}_i^T \mathbf{P}_i) \vec{v}_i - \lambda \cdot \|\vec{v}_i\|_1), \quad \mathbf{P}_{i,j} = \log(S_{i \cap j}) \quad (2)$$

Before defining all terms, the equation comes in three basic parts. First, the principal decomposition depends on the covariance $\mathbf{C} (N_{ROI} \times N_{ROI})$ between mean pairwise mean regional timeseries balanced with a prior \mathbf{P} with an initial belief θ . Next, $\lambda \cdot \|\vec{v}_i\|_1$ imposes the L_1 sparsity with weight λ . Finally, the prior \mathbf{P} is a reformulation of the SC matrix into a matrix where the rows correspond to the individual regions and the columns correspond to a larger network each region can be grouped into. Term by term, \vec{v}_i^* is the structural-connectivity-informed sparse principal component. \vec{v}_i is the i^{th} principal component as we iteratively find each sparse component. \mathbf{P} is the prior matrix derived from the structural connectivity. \mathbf{C} is the covariance matrix between mean regional timeseries. And θ is a scalar which governs

the strength of the prior \mathbf{P} . The prior is constructed from the logarithm of an intermediate matrix $S_{i \cap j}$, which itself is calculated from the structural connectivity matrix. $S_{i \cap j}$ is a block-averaged version of the original structural connectivity matrix, where each row i corresponds to a specific region of interest (ROI), and each column corresponds to some larger network j . In this case, these larger networks j each are a known resting state network (RSN) consisting of multiple ROIs grouped together. Each element i, j represents the intra and inter RSN connectivity. $S_{i \cap j}$ is the summed set of all streamlines that connect the RSN that ROI i is a subset of to RSN j . $S_{1 \cap 1}$ would correspond to the sum of all streamlines which connect sub-regions of RSN 1, representing intra-RSN connectivity. $S_{1 \cap 2}$ would correspond to the sum of all streamlines which connect any subregion of RSN 1 to RSN 2. For example, if we had 100 regions and 10 identified RSNs, matrix \mathbf{P} has dimensions $N_{RSN} \times N_{ROI} = 10 \times 100$, where each row describes the inter-RSN connectivity of that ROI. Each row of the SC-derived prior matrix \mathbf{P} corresponds to a ‘subnetwork’ of the structural connections, and each column describes which subnetwork a specific ROI belongs to. The prior matrix must have a number of RSNs fewer than the number of regional timeseries to reduce the dimensionality in this formulation of constrained sparse PCA, where the number of components is prespecified by the prior dimension. The regularized, sparse principal components will be used in the low-dimensional GC analysis, and the resulting GC scores per region can then be calculated in **Algorithm 3**.

This approach has three advantages over the standard Granger causal measure. *First*, it incorporates prior information from another MRI imaging modality. *Second*, it reduces the number of measure parameters that must be tuned. In SPGC, only the maximum lag needs be selected for the SPGC method as the prior belief weight (θ in **Equation 2**) is fixed at 1 for all experiments, giving equal weighting to the calculated covariance and the prior. GC with an elastic net requires selection of: 1) an L1/L2 ratio, 2) penalty weight, and 3) testing of multiple lags up to and including the maximum lag. In practice, for a given maximum lag, only 1 model needs to be fit for SPGC, while fitting the standard GC requires dozens of cross-validated models to be fit to properly optimize the lag and regularization parameters. *Third*, SPGC model fitting is faster than standard GC, as the number of variables is lower (number of components rather than all regions).

In our specific analysis, we use the Schaefer functional atlas [32] along with the cerebellum and striatum from the AAL atlas [33]. The Schaefer atlas has the advantage where each ROI is assigned a corresponding coarse and fine RSN label to help us better define our RSN connectivity prior. We generate two SC network priors, one with 18 regions (7 RSNs, subcortical structures, and the left and right hemisphere cerebellar gray matter), as well as a prior matrix with 38 regions (17 RSNs, subcortical structures, and the left and right hemisphere cerebellar gray matter). The coarse (18 region) SC prior encourages functional connections that capture left/right hemisphere connections at a whole RSN level, while the fine SC prior encourages the projection of whole brain functional activity to smaller subsections of structurally connected sub-elements of the larger RSNs. We denote the SPGC approach using the coarser 7 RSN prior $SPGC_{coarse}$ and the SPGC approach using the finer 17 RSN prior $SPGC_{fine}$.

As a baseline of comparison, we also choose to use a PCA projection to a number of components preserving 95% of the variance in the timeseries, analogous to previous work [9, 27–30]. This baseline does not impose the structural connectivity prior. This measure can be computed with **Algorithm 3**, but using a PCA projection rather than a structurally-constrained projection. We will denote this PCA-projected low dimensional Granger scored measure PCA_{GC} .

2.2 Materials

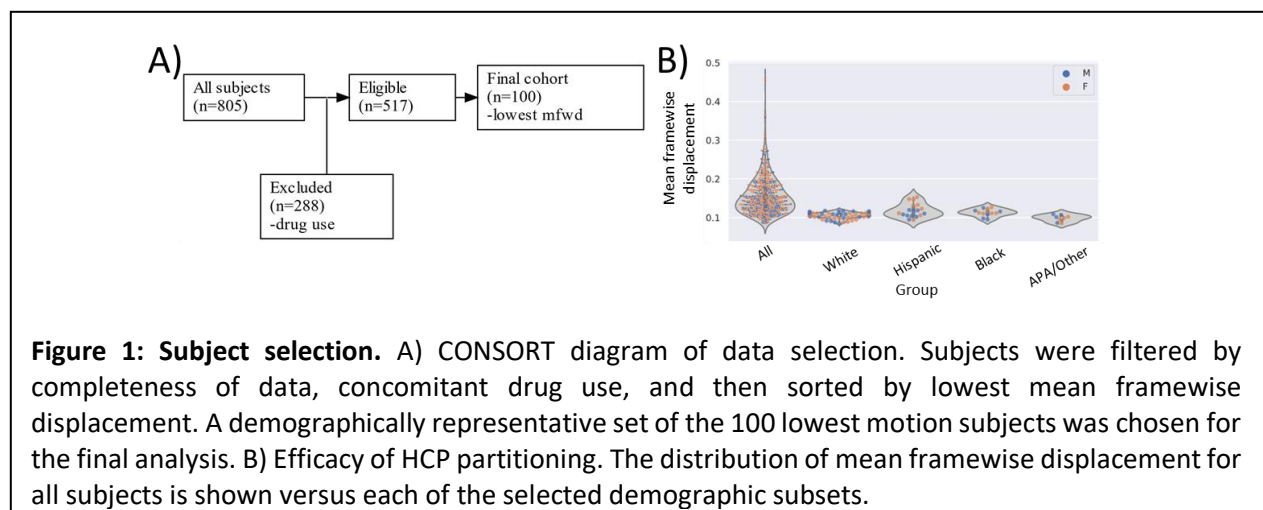
This work uses fMRI data from the Human Connectome Project (HCP) [34] to evaluate the proposed connectivity measures for their reproducibility in producing a consistent connectivity matrix of a single subject over multiple fMRI scans. In particular we use the 4 scans of participants, including on one day: (i) a left-to-right phase-encoded fMRI acquisition and (ii) a right-to-left phase-encoded fMRI acquisition, and on a subsequent day: a repeated (iii) left-to-right and (iv) a right-to left acquisition.

Of all HCP participants, we selected the 805 subjects with all 4 of these fMRI repeat scans and demographic information. From these we excluded subjects with substance use (including alcohol and tobacco), as these are known to confound the reproducibility of longitudinal connectivity. Of the remaining 517 subjects, we selected 100 demographically representative subjects with the least head motion as captured by the lowest mean framewise displacement between fMRI frames. This minimizes potential motion confounds, as head motion can strongly influence connectivity measures with correlated non-neural signal [20, 35]. Subjects were selected to match the demographics of the 2010 USA census data shown in **Table 1** and the CONSORT diagram of data selection is shown in **Figure 1A**. A plot of the mean framewise displacement of the selected subset of 100 subjects versus the 517 initial subjects (**Figure 1B**), confirmed that the chosen subset were indeed low motion compared to the rest of the HCP dataset.

The selected data was processed with the HCP minimal preprocessing pipeline [36]. Mean regional timeseries were extracted with the Schaefer atlas with 100 anatomical regions with additional subcortical regions included [32]. The cerebellum and striatum from the AAL atlas [33] were included, as both structures often contain signals of diagnostic importance and are often missed in standard analysis [37]. The Schaefer atlas is a functional atlas whose regions are defined through the clustering of functional activity in fMRI [32], and this functional atlas was chosen because: 1) a functional atlas tends to capture better functional variability than a purely anatomical atlas, and 2) the Schaefer atlas groups regions into resting-state networks (RSN), which facilitates inter and intra RSN partitioning and analysis.

2.3 Experiment 1: Comparison of reproducibility

The reproducibility of the connectivity methods were compared quantitatively using five different measures. These reproducibility measures can be grouped into linear, nonlinear, and clustering metrics. The linear measurements of reproducibility included: (1) the average root mean square difference of each edge in the connectivity matrix (after z-scoring the connectivity matrix) across runs of the same subject,



and (2) the Pearson’s r between the edges of any 2 pairs of scans of the same subject, averaged over all pairs of scans. The nonlinear measurements of reproducibility included: (3) the average cosine similarity between all edges of any 2 pairs of scans of the same subject, and (4) the two-way random, single score intraclass correlation coefficient (ICC(2,1)) edgewise [20] between any 2 scans of the same subject. Additionally, we calculated a clustering score for each EC or FC metric tested. This clustering score was (5) the Davies-Bouldin (DB) index [38]. This index measures how well each subject is separated from all the subjects after projection to a low dimensional space and a higher index indicates greater separation [39]. A high DB score indicates that a more unique “subject-fingerprint” was identified, capturing elements of connectivity unique to that subject. Finally, given that the reproducibility of some of the EC measures were very similar, we used only a fraction of the timeseries duration to calculate the EC and compared the reliability of the EC measures when using a subset of the full timeseries length. An ideal measure will maintain high reproducibility even using a small portion of the timeseries duration.

2.4 Experiment 2: Comparison of predictability of individuals’ traits: cognitive and physiological

In addition to reproducibility measures, we also took the subset of EC and FC measures that had the highest reproducibility and tested how well the connectivity measures could predict 3 categories of targets: a physiological target, cognitive target, and a combined physiological and cognitive target. The physiologic target chosen from the HCP dataset was *mean arterial blood pressure*, the cognitive target was *fluid intelligence* as measured with the Pennsylvania matrix reasoning test, and the combined physiologic and cognitive target was the *stress and adversity inventory*.

2.4.1 Univariate analysis of effect size

To evaluate how informative the connectivity measures are, first we performed a univariate analysis. Here the effect size per edge was measured with Cohen’s d and compared across the measures with high reproducibility, as measured by Pearson’s r and the individual subject clustering score, to compare predictive information present in the calculated connectivity. An ideal measure will have high reproducibility and high effect size across a variety of predictive tasks.

2.4.2 Multivariate analysis

Univariate analysis does not suffice to show that a connectivity measure is apt to yield accurate multivariable predictions. Therefore, we also used *all edges* with univariate significance $p \leq 0.05$ to form separate multivariable predictive models for each connectivity measure. First, to reduce collinearities, each pair of surviving edges with covariance greater than 0.75 was found and the edge with higher effect size was used. The resulting set of edges was used to predict the targets as in experiment 1 with an elastic net predictor and the predictive power was measured. A 10x5 cross-validation approach was applied. In the 10 fold outer loop the data was stratified by the target measure and 10% of subjects were set aside to test each iteration. For the inner loop 5-fold cross validation loop was performed for hyperparameter optimization where the elastic net’s L1/L2 ratio was tuned with a grid search using ratios from the set {0.1, 0.5, 0.7, 0.9, 0.95, 0.99, 1.0}. The data fidelity to regularization penalty weight α was fitted with coordinate descent, and the model with the lowest mean squared error across the innermost cross validation folds was tested on the 10% test set.

The above procedure was repeated 10 times using Monte Carlo iterations consisting of random permutations of the data as this has been shown to increase the stability of the estimated prediction [40]. The coefficient of determination, R^2 , of the internally fitted model on the held-out data across validation

loops and outer Monte Carlo permutations was recorded. The Bonferroni corrected p-value for the paired one-tailed t-test for the alternative hypothesis that the highest R^2 was greater than each other method's R^2 was reported.

2.4.3 Multi-input, multivariate analysis

To further measure the complementarity of the connectivity measures, an additional modeling test was performed. These secondary modeling approaches test whether edge connectivity measures may contain complementary information and then compares the models built with complimentary features to the base models. A linear mixed effects (LME) model was fit to predict the participants' trait (physiologic, cognitive, or physiological-cognitive) by combining the predictions from several models that each use a single connectivity measure. For example, the predicted mean arterial pressure predicted from partial correlation would be concatenated with the predicted pressure from each other measure of FC into a vector, and that vector of predictions was used to predict mean arterial pressure. If partial correlation contains information that $MLFC_{ERT}$ does not and vice-versa, we would expect the LME model to give significant weight to predictions generated from both partial correlation and $MLFC_{ERT}$. If the partial correlation measures contain information that is redundant with the $MLFC_{ERT}$ measures, we would expect the LME model to give weight only to one of the two FC predictions. Elastic models for each individual FC or EC measure were generated from hyperparameters averaged over the highest cross-validated parameters from the previous 10 fold outer, 5 fold inner procedure outlined in **Section 2.4.2** and refit to all the data. The LME models were fit with a subject-specific intercept and group level slope per (**Equation 3**).

$$y_{i,j} = \mu_{0,j} + \beta_1 x_{1,j} + \beta_2 x_{2,j} + \dots + \beta_n x_{n,j} + \epsilon_{i,j} \quad (3)$$

The predicted trait for subject j , trial i ($y_{i,j}$) is a function of the subject-specific intercept ($\mu_{0,j}$) and the group level slopes (β_n). Each predictor ($x_{i,j}$) is the predicted value of the trait (e.g. predicted mean arterial pressure, stress, etc.) from the elastic models trained from a single measure (e.g. Partial Correlation). The fitted LME coefficients with $p \leq 0.05$ and magnitude greater than 10% of the maximum coefficient magnitude were considered to contain complimentary information in the predictions. This gave a subset of complimentary FC or EC features that could then be used in another multi-input, multivariate elastic net model. This secondary model with complimentary features was also fit with the same 10x5 cross-validation strategy. The secondary elastic model with complimentary features was compared to the original models, to see the magnitude of the benefit of combining the complimentary features.

3 Results

3.1 Experiment 1: Comparison of reproducibility

3.1.1 Comparison of the reproducibility of functional connectivity

The reproducibility of six functional connectivity metrics: 1) Pearson's Correlation based connectivity, 2) partial correlation connectivity, 3) spectral GC connectivity, and MLFC based connectivity 4) with XGBoost, 5) with extremely random trees, and 6) with a radial basis function support vector regressor was quantified with five measures. These measures included: Pearson's r , Root Mean Square Error (RMSE), ICC, cosine similarity, and the *ease of separability* (DB clustering score) as described in **Section 2.3**. Results of this comparison are shown in **Table 2** with the 5 right most columns showing the mean reproducibility and 95% confidence interval. The highest reproducibility in a given column is in boldface and significant

Table 2: Comparison of the reproducibility of the six FC methods including proposed (gray shaded) and traditional (nonshaded) functional connectivity measures. The section of this article where the measure is described is indicated in the Section column. The best performing methods in each metric are shown in **boldface**. Statistically significant differences from the best performing method after FDR correction at 5% are indicated with *. *Correlation*=correlation, *PartialCorr*=partial correlation, *SpectGC*=spectral Granger causality/instantaneous spectral density, *MLFC_{ERT}*=machine learning functional connectivity using an extremely random trees predictor, *MLFC_{SVM}*=machine learning functional connectivity using a support vector regressor, *MLFC_{XGB}*=machine learning functional connectivity using an XGBoost model.

FC measure (ours)	Section	Linear		Nonlinear		Clustering
		Pearson's r	RMSE	ICC(2,1)	Cosine similarity	Clustering DB Score
<i>Correlation</i>	1	0.40 ± 0.00*	0.70 ± 0.02*	0.43 ± 0.0	0.75 ± 0.01	10.5 ± 1.0*
<i>PartialCorr</i>	1	0.44 ± 0.00*	0.49 ± 0.00*	0.07 ± 0.00*	0.88 ± 0.00*	0.23 ± 0.01
<i>SpectGC</i>	1	0.31 ± 0.01*	0.92 ± 0.02*	0.29 ± 0.00*	0.57 ± 0.02*	13.2 ± 1.0*
<i>MLFC_{ERT}</i>	2.1.1	0.42 ± 0.00*	0.56 ± 0.01*	0.31 ± 0.00*	0.84 ± 0.01*	5.55 ± 0.55*
<i>MLFC_{SVM}</i>	2.1.1	0.35 ± 0.00*	0.79 ± 0.01*	0.27 ± 0.00*	0.68 ± 0.01*	8.00 ± 0.97*
<i>MLFC_{XGB}</i>	2.1.1	0.46 ± 0.00	0.40 ± 0.00	0.06 ± 0.00*	0.93 ± 0.00*	3.14 ± 0.30*

differences (FDR corrected p -value < 0.05) between the bold result and each other entry in that column is denoted with an asterisk, *. The proposed metrics are distinguished with a grey background. Of all the FC metrics, the proposed *MLFC_{XGB}* connectivity had the highest Pearson's r and cosine similarity, as well as the lowest RMSE. Partial correlation connectivity had the best (lowest) DB index while, correlation based connectivity had a higher ICC than any other metric, but is also less sparse than other metrics which may artificially inflate this measure. The RMSE is a suboptimal metric of reproducibility across multiple metric types due to the different distributions and sparsity of the FC metrics, but is shown in order to facilitate

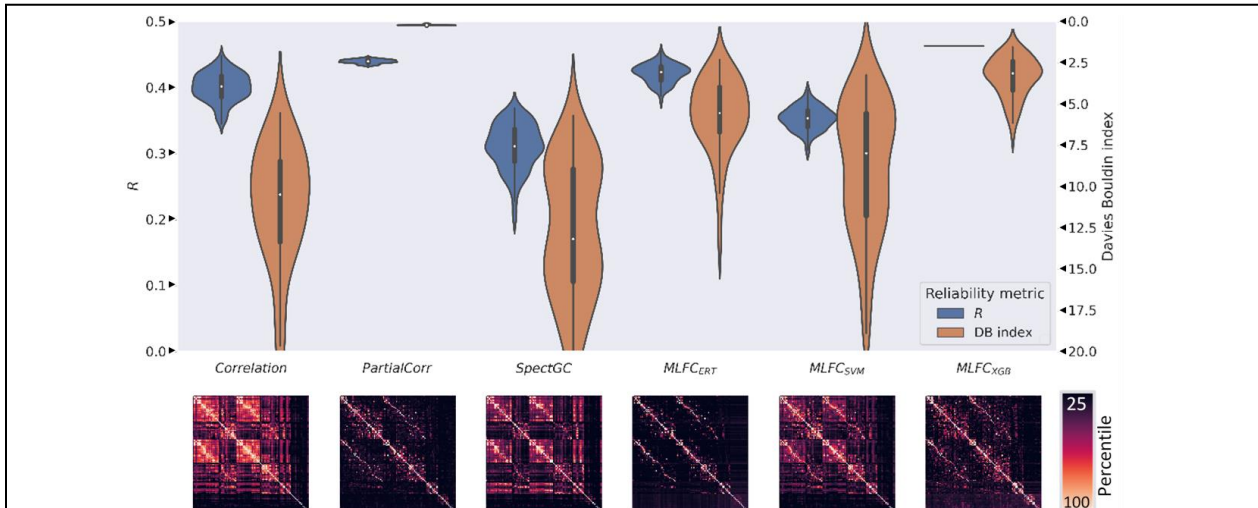


Figure 2: Reproducibility of functional connectivity measures across repeat scans as measured by Pearson's r and Davies Bouldin Index. This figure shows the reproducibility as measured by Pearson's r and DB clustering score for every pair of FC matrices in the four-scan set per subject. Superior reproducibility for both metrics is found at the top of the graph. The distributions of the reproducibility metrics are shown, with the mean FC matrix displayed on the x axis.

comparisons to the literature. Pearson's r which is less susceptible to scale variations and sparsity, and the DB clustering score, which looks at a measure of subject identifiability, were chosen as more reproducible measures for further analysis. A comparison of the six FC methods along these two metrics is shown in **Figure 2**. Under the X axis, the mean connectivity matrix is shown which is computed across all subject scans for each method. **Supplementary Figure S1** describes the consistent ordering of the anatomy and RSNs across the columns and rows in each matrix. The proposed $MLFC_{XGB}$ with XGBoost connectivity metric (right) had the highest reproducibility by most measures (**bold** in **Table 2**) including Pearson's r , while partial correlation had the second highest for most measures except DB score, for which it had the highest. This suggests conditioning the connectivity between two nodes on all other node activity is crucial to maintain reproducibility.

3.1.2 Comparison of the reproducibility of effective connectivity

The effective connectivity measures were evaluated with Pearson's r , RMSE, ICC, cosine similarity, and the ease of separability via the DB score, as described in **Section 2.3**. The results of this comparison are shown in **Table 3**. Significant differences are denoted with an asterisk and the most reproducible measure in each column is boldfaced. The proposed metrics are shown with a grey background shading. We note that the ICC metric for measuring the reproducibility of the GC connectivity measures is influenced by the sparsity of the connectivity measure. The proposed $MLEC_{ERT}$ connectivity with extremely random trees predictor

Table 3: Comparison of the reproducibility of the six EC methods including proposed (gray shaded) and traditional (nonshaded) functional connectivity measures. The section where the measure is described is indicated in the Section column. The best performing methods in each metric are shown in **boldface**. Statistically significant differences from the best performing method after FDR correction at 5% are indicated with *.

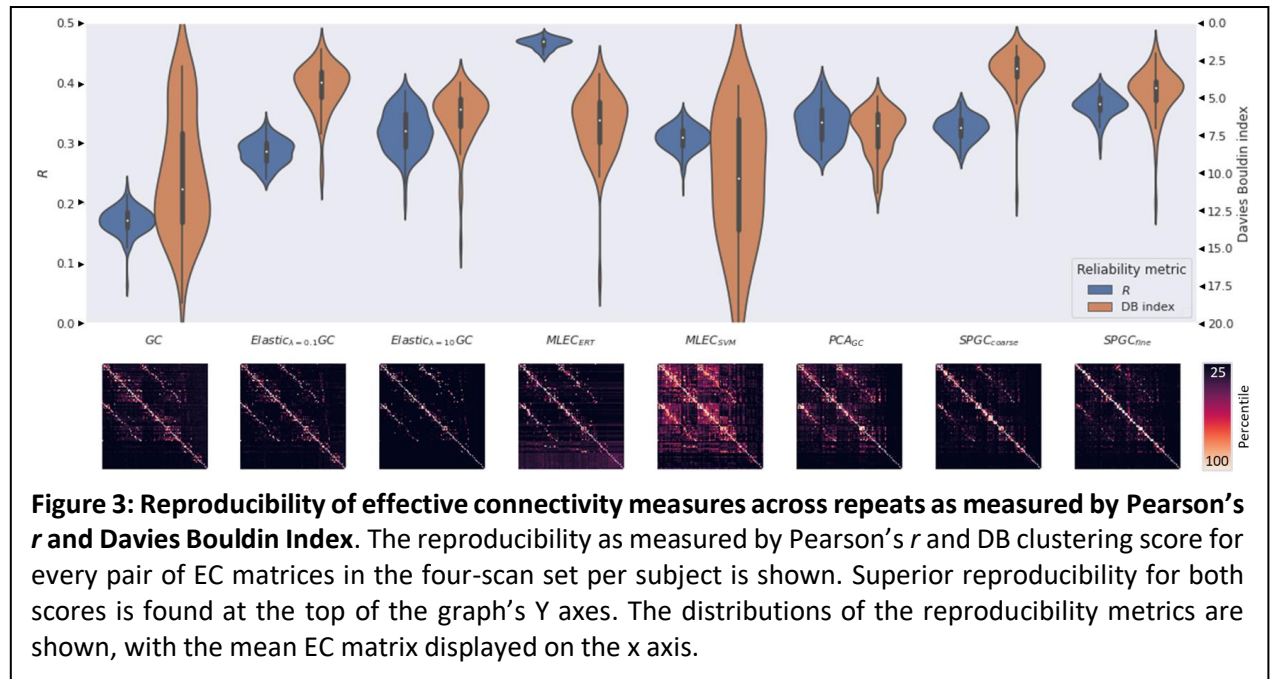
GC = Granger causality measured with an unpenalized MVAR model, $Elastic_{\lambda=0.01} GC$ = Granger causality measured with an elastic MVAR model with equal L_1 and L_2 penalties and a regularization parameter of 0.01, $Elastic_{\lambda=10} GC$ = Granger causality measured with an elastic MVAR model with equal L_1 and L_2 penalties and a regularization parameter of 10, $MLEC_{ERT}$ = Machine learning effective connectivity using an extremely random trees predictor, $MLEC_{SVM}$ = Machine learning effective connectivity using a support vector machine regressor, PCA_{GC} = low dimensional Granger causality measured with an MVAR model in PCA space, $SPGC_{coarse}$ = structurally projected Granger causality measured with an MVAR model in the low dimensional space informed by the structural prior using 7 resting state network sub-parcelations, $SPGC_{fine}$ = structurally projected Granger causality measured with an MVAR model in the low dimensional space informed by the structural prior using 17 resting state network sub-parcelations.

EC measure (ours)	Section	Linear		Nonlinear		Clustering
		Pearson's r	RMSE	ICC(2,1)	Cosine similarity	Clustering DB Score
GC	2.1.2	$0.17 \pm 0.00^*$	$1.15 \pm 0.01^*$	$0.10 \pm 0.00^*$	$0.34 \pm 0.01^*$	$11.0 \pm 1.1^*$
$Elastic_{\lambda=0.01} GC$	2.1.2	$0.29 \pm 0.00^*$	$0.93 \pm 0.01^*$	$0.01 \pm 0.00^*$	$0.57 \pm 0.01^*$	$3.97 \pm 0.39^*$
$Elastic_{\lambda=10} GC$	2.1.2	$0.32 \pm 0.01^*$	$0.85 \pm 0.02^*$	$0.00 \pm 0.00^*$	$0.64 \pm 0.01^*$	$5.78 \pm 0.44^*$
$MLEC_{ERT}$	2.1.3	0.47 ± 0.00	0.37 ± 0.01	0.39 ± 0.00	0.93 ± 0.00	$6.50 \pm 0.52^*$
$MLEC_{SVM}$	2.1.3	$0.31 \pm 0.00^*$	$0.90 \pm 0.01^*$	$0.22 \pm 0.00^*$	$0.59 \pm 0.01^*$	$10.4 \pm 1.4^*$
PCA_{GC}	2.1.4	$0.33 \pm 0.01^*$	$0.82 \pm 0.02^*$	$0.15 \pm 0.00^*$	$0.67 \pm 0.01^*$	$6.84 \pm 0.36^*$
$SPGC_{coarse}$	2.1.4	$0.32 \pm 0.00^*$	$0.84 \pm 0.01^*$	$0.07 \pm 0.00^*$	$0.65 \pm 0.01^*$	3.00 ± 0.36
$SPGC_{fine}$	2.1.4	$0.36 \pm 0.00^*$	$0.76 \pm 0.01^*$	$0.06 \pm 0.00^*$	$0.73 \pm 0.01^*$	$4.32 \pm 0.39^*$

outperformed all other traditional and proposed methods across *all* metrics except clustering, where it provided a respectable performance close to the median among the tested methods. The proposed $MLEC_{ERT}$ connectivity outperformed the proposed $MLEC_{SVM}$ with SVM implementation across all reproducibility measures, suggesting superiority of the ERT based predictor for this connectivity measure.

The regularized GC connectivity measures from the elastic multivariate autoregressive model (MVAR) performed significantly better than the unregularized GC measure. The higher elastic penalty ($\lambda = 10$) increased Pearson's r relative to the lower elastic penalty ($\lambda = 0.1$), and the lower elastic penalty had a superior cluster separability. The proposed structurally projected GC method, $SPGC_{fine}$, attained greater reproducibility than either elastic or PCA_{GC} connectivity measures in its DB score, and was slightly better in all other measures of reproducibility except ICC(2,1). To further understand the differences between the Granger-causal connectivity metrics, we quantified the stability of these measures as a function of the amount of scan time (fMRI timeseries length) used to measure the causal connectivity. Notably, $SPGC_{fine}$ using 50% of the initial timeseries has a higher reproducibility than the Elastic GC or PCA_{GC} methods using 100% of the timeseries. Full results of the GC comparison are described in **Supplementary Figure S2**. The higher performances of the $SPGC_{fine}$ approach in this supplementary analysis relative to the PCA_{GC} approach indicate that the imposed prior and the low dimensional projection create a regularization scheme that is more consistent between scans of the same subject than another lower dimensional projection. Perhaps more importantly, the $SPGC_{fine}$ projection is more stable when given shorter timeseries than the other competing GC approaches.

The distributions of Pearson's r and the clustering score for each of the EC metrics are shown in **Figure 3**. This view manifests the clearly superior performance of $MLEC_{ERT}$ connectivity along the Pearson's r metric as well as the reasonable clustering performance. Below each measure is the mean connectivity matrix across all subject scans for each measure. **Supplementary Figure S1** describes the ordering of the anatomy and RSNs across the columns and rows in each matrix.



3.2 Experiment 2: Comparison of predictability of individual's traits: cognitive and physiological

3.2.1 Comparison of trait predictability using the proposed functional connectivity measures

The ability of the connectivity metrics to predict subject level traits was evaluated in the second experiment. The most reproducible FC proposed measures ($MLFC_{ERT}$ and $MLFC_{XGB}$) were compared to more traditional methods of FC, namely correlation and partial correlation based connectivity (**Figure 4**). We first performed the univariate analysis of effect size per FC edge as described in **Section 2.4.1**. **Figure 4A** shows the effect size of the top 50 FC edges in predicting mean arterial pressure, **Figure 4B** shows the effect size of the top 50 edges in predicting stress, and **Figure 4C** shows the effect size of the top 50 edges in predicting fluid intelligence. The effect sizes of the different methods are comparable for the different predictions except for fluid intelligence, where Correlation and $MLFC_{ERT}$ gave superior performance.

Next, we performed the multivariate analysis described in **Section 2.4.2** in which we combined multiple edges into one model so that we can quantify whether the edges contain complementary information and which measures contain the largest total information about our prediction targets: arterial pressure, stress, and intelligence. **Figure 4D** shows the R^2 on the held out test data using 10 fold cross-validation nested within 10 Monte Carlo permutations. For all three of our cognitive and physiological targets, multivariate connectivity from $MLFC_{XGB}$ gave the top performance, followed closely behind by Partial

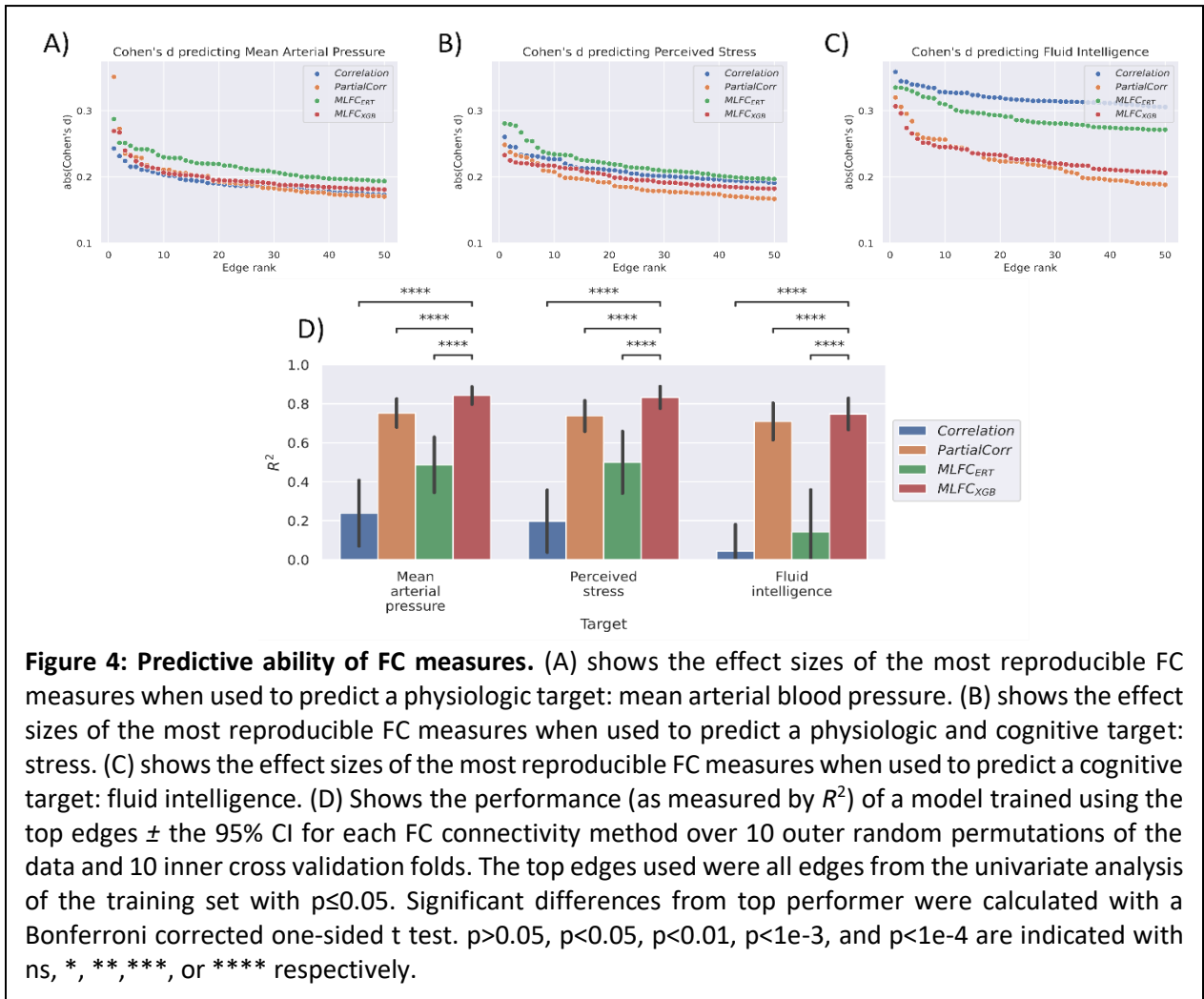


Table 4: Complementarity of EC and FC measures. For each set of EC and FC measures, the predicted scores from the elastic-net predictions were fed into a secondary LME model with subject-specific intercepts and group level slopes. This tested for complimentary information contained in the predictions. Those predictions using connectivity metrics were considered to contain complimentary information if the fitted coefficient had a p-value ≤ 0.05 and a magnitude greater than or equal to 10% of the maximum coefficient magnitude. The coefficients are displayed below, with p values in parentheses. Complimentary sets of connectivity features are indicated with boldface.

Prediction Target	Functional connectivity measure			
	<i>Correlation</i>	<i>PartialCorr</i>	<i>MLFC_{ERT}</i>	<i>MLFC_{XGB}</i>
Mean arterial pressure	-0.02 (0.00)	0.10 (0.00)	0.02 (0.07)	0.92 (0.00)
Perceived stress	-0.02 (0.05)	0.06 (0.00)	0.01 (0.14)	0.97 (0.00)
Fluid intelligence	-0.02 (0.00)	0.00 (0.94)	-0.01 (0.01)	1.03 (0.00)

Prediction Target	Effective connectivity measure			
	<i>GC</i>	<i>Elastic_{$\lambda=0.1$}GC</i>	<i>PCAGC</i>	<i>SPGC_{fine}</i>
Mean arterial pressure	-0.05 (0.17)	0.74 (0.00)	0.08 (0.00)	0.24 (0.00)
Fluid intelligence	-0.35 (0.49)	0.31 (0.00)	0.52 (0.00)	0.24 (0.00)
Perceived stress	0.24 (0.00)	0.22 (0.00)	0.63 (0.00)	0.28 (0.00)

correlation. $MLFC_{ERT}$ and correlation were distant 3rd and 4th place finishers. Using the elasticnet predictions themselves as input to a second level LME model allowed to determine which predictions were complementary (**Table 4**). However, we found that this combining the complimentary features did not provide a statistically significant improvement upon the target predictions. We found that $MLFC_{XGB}$ contained the information present in the other measures in all cases except mean arterial pressure. For that target, $MLFC_{XGB}$ and partial correlation contained complimentary information. The results from **Figure 4** and **Table 4** suggest that the boosting method of $MLFC_{XGB}$ is particularly well-suited to regularize and discover a stable set of connectivity features, perhaps because of the multiple-bagging approach used to handle multicollinearity.

3.2.2 Comparison of trait predictability using proposed effective connectivity measures

The predictive ability of the different *effective* connectivity metrics were also evaluated in the second experiment. The traditional EC measures of GC, regularized GC with an elastic penalty, and PCA_{GC} were compared to the most reproducible proposed metrics, $MLEC_{ERT}$ with the extremely random trees predictor and $SPGC$. **Figure 5A-C** shows the results from this univariate analysis, outlined in **Section 2.4.1**. In general we observed that the highest Cohen's d was attained for connections measured with PCA_{GC} (red) and $MLFC_{ERT}$ (green) followed by $SPGC$ (purple). **Figure 5D** shows the performance of multivariate predictive models trained on a set of all edges who had a univariate p-value ≤ 0.05 . Each multivariate model was an elastic net model evaluated on 10 fold cross validation nested within 10 external Monte Carlo permutations. The proposed SPGC method (purple) tended explained the most variance, followed by CA_{GC} (red), then $MLEC_{ERT}$ (green). Overall, the $MLEC_{ERT}$ and PCA_{GC} approaches yielded pairwise connections (edges) with the highest Cohen's d and the $SPGC$ approach performing next highest. The unpenalized GC approach (blue) performed poorly across all tasks.

These multivariate trait predictive elastic net models (**Figure 5D**) revealed that the $SPGC$ set of edges tended to contain more total information than the connections computed with the remaining connectivity methods, and achieving the highest performance predicting arterial pressure and stress. In close second

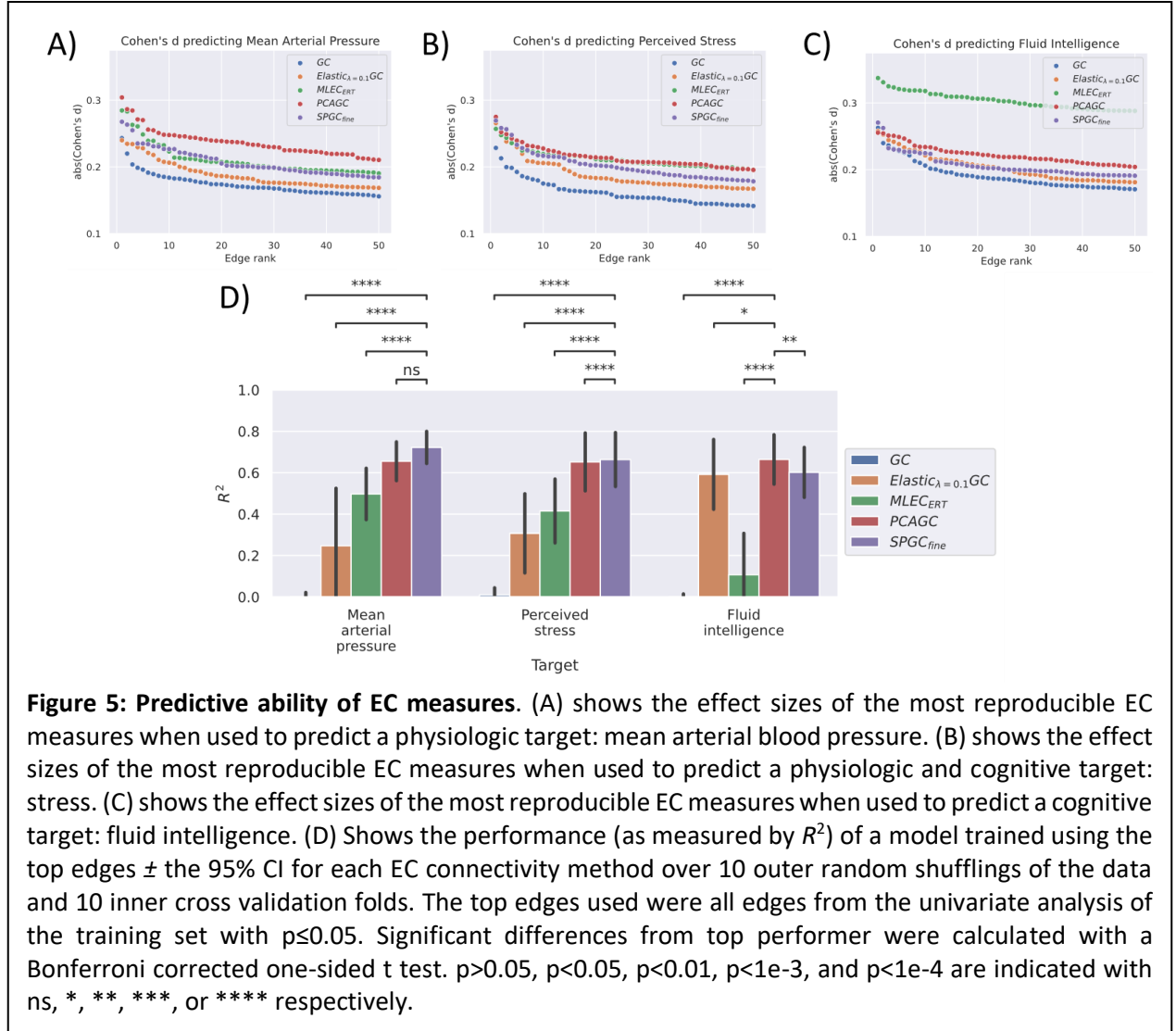


Figure 5: Predictive ability of EC measures. (A) shows the effect sizes of the most reproducible EC measures when used to predict a physiologic target: mean arterial blood pressure. (B) shows the effect sizes of the most reproducible EC measures when used to predict a physiologic and cognitive target: stress. (C) shows the effect sizes of the most reproducible EC measures when used to predict a cognitive target: fluid intelligence. (D) Shows the performance (as measured by R^2) of a model trained using the top edges \pm the 95% CI for each EC connectivity method over 10 outer random shufflings of the data and 10 inner cross validation folds. The top edges used were all edges from the univariate analysis of the training set with $p \leq 0.05$. Significant differences from top performer were calculated with a Bonferroni corrected one-sided t test. $p > 0.05$, $p < 0.05$, $p < 0.01$, $p < 1e-3$, and $p < 1e-4$ are indicated with ns, *, **, ***, or **** respectively.

place was the $PCAGC$ connectivity measure, achieving the highest performance predictive fluid intelligence.

We also performed the multi-input analysis described in **Section 2.4.3** to test complementarity across the EC measures using an LME model. These results are shown in **Table 4** (bottom). We observe that $SPGC$, $PCAGC$, and $Elastic_{\lambda=0.1}GC$ contained complimentary information for all prediction targets. However, we found that this combining the complimentary features did not provide a statistically significant improvement upon the target predictions. Taken together, these results indicate that the regularized causal measures, either from a low dimensional projection or from an elastic penalty, all extract different information depending on the regularization scheme used. Furthermore, the cross-prediction comparison indicates that the single connectivity feature most apt to make a given prediction is somewhat problem specific, but $SPGC$ and $PCAGC$ are well-suited to the variety of prediction tasks examined here.

4 Discussion

Of the various *functional connectivity* measures, $MLFC_{XGB}$ had the highest reproducibility across most metrics. The overall predictive power to predict mean arterial pressure, stress, and fluid intelligence using

the multivariate models was highest for $MLFC_{XGB}$, and second highest for partial correlation. $MLFC_{ERT}$ and $MLFC_{SVM}$ performed worse than $MLFC_{XGB}$. Additionally, our separate analysis of complementarity using second level LME models revealed that the $MLFC_{XGB}$ approach contained most of the information present in the other modalities. Due to the high predictive power, reproducibility, and information content, we suggest that $MLFC_{XGB}$ be used as the functional connectivity metric of choice on larger datasets and if there is not enough data to effectively fit the $MLFC_{XGB}$ across subjects, then we recommend the use of partial correlation based functional connectivity.

Of the various *effective connectivity* measures, the proposed $MLEC_{ERT}$ methodology performed near-universally better in reproducibility than any other metric, but performed suboptimally in the predictive power analysis, suggesting the presence of strong intra-edge correlation and redundant information. However, our proposed structurally projected GC methodology ($SPGC$) performed second highest in reproducibility *and was also* the most predictive connectivity feature set in two of our three prediction models. Furthermore, our analysis of reproducibility with only part of the initial timeseries showed that the $SPGC_{fine}$ measure maintained its high reproducibility even when given less and less time points of fMRI data. Our complementarity analysis using second level LME models, showed that each of the top EC methods contained information complimentary to each other. Collectively these results indicate that the incorporation of a structural prior to the $SPGC_{fine}$ measure appropriately constrained the calculated GC scores to a more reliable domain with higher predictive power and reproducibility than a standard PCA projection scheme. If a dMRI structural constraint is available per subject in a given dataset or if an ensembled prior from multiple subjects is appropriate, we recommend the use of $SPGC_{fine}$ as the EC metric of choice. If appropriate dMRI priors are not readily available (for example, in cases of traumatic brain injury or in children), we recommend using either the $MLEC_{ERT}$ approach for capturing nonlinear EC connectivity to maximize reproducibility, and recommend PCA_{GC} if predictive power is prioritized over reproducibility.

Prior literature focused on reproducibility of functional connectivity, either Pearson’s r or, less commonly, partial correlation [2, 3, 20, 22–24, 41–45]. Measures of reproducibility can be highly confounded (usually inflated) by motion, so we performed careful processing and selection of data to minimize this confound [20]. We think that our somewhat lower estimates of reproducibility of FC measures relative to some reports in the literature is largely related to our strict motion cutoffs limiting correlation between signals due to motion, which is supported by previous reviews of connectivity [20]. The aforementioned prior research characterizes reproducibility of correlation and partial correlation well, with a limited set of reliability metrics, primarily the intraclass correlation coefficient (ICC) or R^2 . However, a more thorough characterization of reproducibility using multiple metrics simultaneously (ICC, R^2 , cosine similarity, etc.) better identifies connectivity measures that consistently make accurate predictions across multiple predictive targets (intelligence, vascular health, etc.) [21–23]. Therefore, we used multiple measures of reproducibility to characterize both EC and FC measures.

Machine learning feature importance metrics are also used in [26] which can be considered a special case of the generalized framework for MLFC presented in our work. Our framework is capable of handling additional model types and is systematically normalized. We demonstrate our framework generalizability using multiple predictive models including SVM, ERT, and XGB models and using our framework for both FC and EC, while the focus in [26] was on FC. We also evaluate the reproducibility of the proposed models, which is absent from the prior literature and which is the focus of this work.

Beyond these studies examining reproducibility in FC, examinations of the reproducibility of EC measures have been limited to bivariate GC, which is a Granger causal estimate using only pairs of regional timeseries, rather than the more comprehensive multivariate estimates using all regional timeseries (as employed in this paper) [3]. There is thus an egregious gap on the study of reproducibility of EC measures beyond this bivariate GC analysis, a gap which this research addresses. Furthermore, although many studies do not characterize performance, reproducibility is necessary but insufficient quality of a good neuroimaging predictor [21–24]. Our analysis of predictive power over multiple tasks addresses this additional gap in current research.

There are several limitations of this research. *First*, the measurement of reproducibility across different connectivity types can be problematic when the distribution of connectivity values is concentrated to a few values. For example, an elastic GC connectivity where the λ penalty is extremely high can have 99% values of 0 connectivity, and the remaining nonzero connections can be uniformly distributed on a logarithmic scale, bounded from 0 to ∞ . On the other hand, correlative connectivity values are bounded to $[-1,1]$ and tend to be normally distributed. By using multiple metrics of comparison including many measures of both reproducibility and predictive power, we increase confidence in the relative usefulness of the analyzed measures. However, additional reproducibility metrics could have been explored. Summary graph measures may exhibit useful predictive properties and reliability, but the differing sparsity between methods needs to be addressed to make this comparison. The *second* limitation is that measures of connectivity and reproducibility can be dependent upon preprocessing decisions. Future studies could explore the dependency of FC and EC measures to denoising, global signal regression, and choice of atlas.

This study proposes several novel measures of functional and effective connectivity to address weaknesses in traditional measures. This study compared the proposed measures to traditional measures along the highly sought after qualities of *reproducibility* and *predictive power* across multiple relevant neurobiological domains. The proposed measures produced higher measures of reproducibility and were found to be more predictive across an array of biologically relevant targets, including a physiologic target, cognitive target, and combined physiologic and cognitive target. These contributions hold significant potential to further the development of tools to characterize the human connectome in health and disease and make meaningful individualized predictions of neuropsychological and neurobiological states.

5 Acknowledgements

Special thanks Dr. Prapti Modi, PhD, and Dr. Daniel Heitjan, PhD, for providing additional feedback and editing during the writing of this manuscript. Cooper Mellema was supported by NIH NINDS F31 fellowship NS115348. Albert Montillo was supported by NIH NIA R01AG059288, NIH NCI U01 CA207091, the King Foundation, and the Lyda Hill Foundation. The authors declare no competing interests.

6 Materials and ethics statement

To facilitate reuse and extension, the authors are pleased to provide full source code for methods and analyses of this manuscript at the time of publication. Datasets used for analysis during this study are available from the human connectome project (<http://www.humanconnectomeproject.org/>). The data used for this study were deidentified in accordance with NIH guidelines, HIPPA guidelines, and according to the ethical standards set forth in the NIH Human Connectome Project. All data was gathered with informed consent from all participants.

7 References

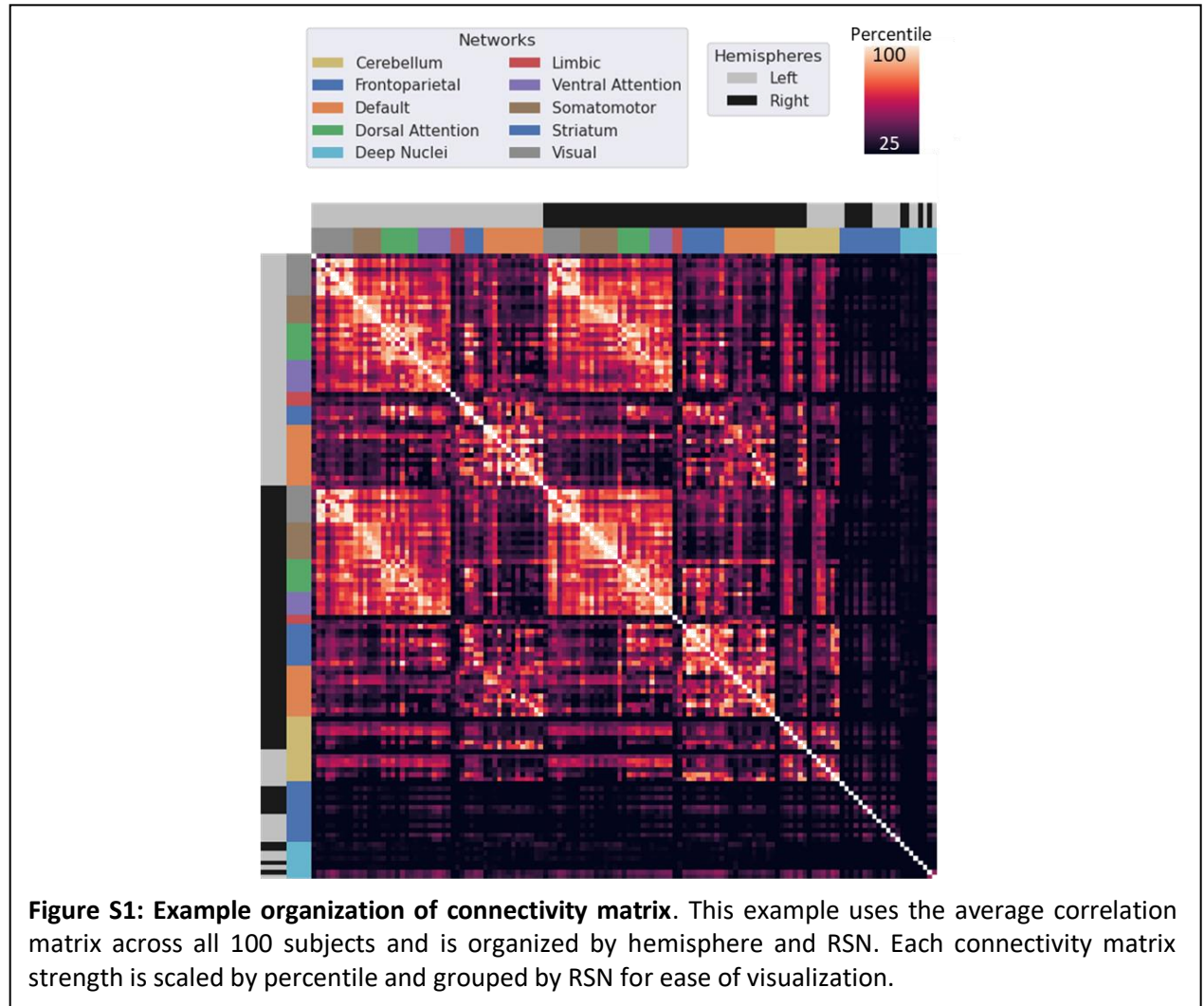
- [1] J. B. Rowe, "Connectivity Analysis is Essential to Understand Neurological Disorders," *Frontiers in systems neuroscience*, vol. 4, 2010, doi: 10.3389/fnsys.2010.00144.
- [2] M. Andellini, V. Cannatà, S. Gazzellini, B. Bernardi, and A. Napolitano, "Test-retest reliability of graph metrics of resting state MRI functional brain networks: A review," *Journal of neuroscience methods*, vol. 253, pp. 183–192, 2015, doi: 10.1016/j.jneumeth.2015.05.020.
- [3] M. Fiecas, H. Ombao, D. van Lunen, R. Baumgartner, A. Coimbra, and D. Feng, "Quantifying temporal correlations: a test-retest evaluation of functional connectivity in resting-state fMRI," *NeuroImage*, vol. 65, pp. 231–241, 2013, doi: 10.1016/j.neuroimage.2012.09.052.
- [4] Büchel, C. and Friston, K. J, *Effective connectivity and neuroimaging*: Institute of Neurology, Wellcome Department of Cognitive Neurology, London, UK., 1997. [Online]. Available: <http://www.fil.ion.ucl.ac.uk/spm/course/notes97/Ch6.pdf>
- [5] K. A. Smitha *et al.*, "Resting state fMRI: A review on methods in resting state connectivity analysis and resting state networks," *Neuroradiology Journal*, vol. 30, no. 4, pp. 305–317, 2017, doi: 10.1177/1971400917697342.
- [6] J. D. Cohen *et al.*, "Computational approaches to fMRI analysis," *Nature neuroscience*, vol. 20, no. 3, pp. 304–313, 2017, doi: 10.1038/nn.4499.
- [7] C. W. J. Granger, "Investigating Causal Relations by Econometric Models and Cross-spectral Methods," *Econometrica*, vol. 37, no. 3, pp. 424–438, 1969.
- [8] Anas Z. Abidin, Adorma M. DSouza, Axel Wismuller, "Detecting connectivity changes in autism spectrum disorder using large-scale Granger causality," *SPIE, Proceedings*, no. 10949, 2109.
- [9] U. Chockanathan, A. M. DSouza, A. Z. Abidin, G. Schifitto, and A. Wismüller, "Automated diagnosis of HIV-associated neurocognitive disorders using large-scale Granger causality analysis of resting-state functional MRI," *Computers in biology and medicine*, vol. 106, pp. 24–30, 2019, doi: 10.1016/j.combiomed.2019.01.006.
- [10] E. Spencer *et al.*, "A procedure to increase the power of Granger-causal analysis through temporal smoothing," *Journal of neuroscience methods*, vol. 308, pp. 48–61, 2018, doi: 10.1016/j.jneumeth.2018.07.010.
- [11] H.-J. Park, K. J. Friston, C. Pae, B. Park, and A. Razi, "Dynamic effective connectivity in resting state fMRI," *NeuroImage*, vol. 180, Pt B, pp. 594–608, 2018, doi: 10.1016/j.neuroimage.2017.11.033.
- [12] K. J. Friston *et al.*, "Dynamic causal modelling revisited," *NeuroImage*, 2017, doi: 10.1016/j.neuroimage.2017.02.045.
- [13] N. Z. Bielczyk, S. Uithol, T. van Mourik, P. Anderson, J. C. Glennon, and J. K. Buitelaar, "Disentangling causal webs in the brain using functional magnetic resonance imaging: A review of current approaches," *Network neuroscience (Cambridge, Mass.)*, vol. 3, no. 2, pp. 237–273, 2019, doi: 10.1162/netn_a_00062.
- [14] M. Ding, Y. Chen, S.L. Bressler, Ed., *Handbook of Time Series Analysis: Granger causality: basic theory and application to neuroscience*: Wiley-VCH Verlag, 2006.
- [15] H. Huang and M. Ding, "Linking Functional Connectivity and Structural Connectivity Quantitatively: A Comparison of Methods," *Brain connectivity*, vol. 6, no. 2, pp. 99–108, 2016, doi: 10.1089/brain.2015.0382.
- [16] L. A. Maglanoc *et al.*, "Multimodal fusion of structural and functional brain imaging in depression using linked independent component analysis," *Human brain mapping*, vol. 41, no. 1, pp. 241–255, 2020, doi: 10.1002/hbm.24802.
- [17] G. I. Allen and M. Weylandt, "Sparse and Functional Principal Components Analysis," pp. 11–16, 2019, doi: 10.1109/DSW.2019.8755778.
- [18] J. R. Manning *et al.*, "A probabilistic approach to discovering dynamic full-brain functional connectivity patterns," *NeuroImage*, vol. 180, Pt A, pp. 243–252, 2018, doi: 10.1016/j.neuroimage.2018.01.071.
- [19] K. Dillon, V. Calhoun, and Y.-P. Wang, "A robust sparse-modeling framework for estimating schizophrenia biomarkers from fMRI," *Journal of neuroscience methods*, vol. 276, pp. 46–55, 2017, doi: 10.1016/j.jneumeth.2016.11.005.
- [20] S. Noble, D. Scheinost, and R. T. Constable, "A decade of test-retest reliability of functional connectivity: A systematic review and meta-analysis," *NeuroImage*, vol. 203, p. 116157, 2019, doi: 10.1016/j.neuroimage.2019.116157.
- [21] L. Waller *et al.*, "Evaluating the replicability, specificity, and generalizability of connectome fingerprints," *NeuroImage*, vol. 158, pp. 371–377, 2017, doi: 10.1016/j.neuroimage.2017.07.016.
- [22] M. Termenon, A. Jaillard, C. Delon-Martin, and S. Achard, "Reliability of graph analysis of resting state fMRI using test-retest dataset from the Human Connectome Project," *NeuroImage*, vol. 142, pp. 172–187, 2016, doi: 10.1016/j.neuroimage.2016.05.062.
- [23] S. Noble *et al.*, "Multisite reliability of MR-based functional connectivity," *NeuroImage*, vol. 146, pp. 959–970, 2017, doi: 10.1016/j.neuroimage.2016.10.020.
- [24] S. Noble, M. N. Spann, F. Tokoglu, X. Shen, R. T. Constable, and D. Scheinost, "Influences on the Test-Retest Reliability of Functional Connectivity MRI and its Relationship with Behavioral Utility," *Cerebral cortex*, vol. 27, no. 11, pp. 5415–5429, 2017, doi: 10.1093/cercor/bhx230.
- [25] Q. Luo *et al.*, "Spatio-temporal Granger causality: a new framework," *NeuroImage*, vol. 79, pp. 241–263, 2013, doi: 10.1016/j.neuroimage.2013.04.091.
- [26] G. K. Murugesan *et al.*, "BrainNET: Inference of Brain Network Topology Using Machine Learning," *Brain connectivity*, vol. 10, no. 8, pp. 422–435, 2020, doi: 10.1089/brain.2020.0745.

- [27] T. Chen and C. Guestrin, "XGBoost: A Scalable Tree Boosting System," in *Proceedings of the 22nd ACM SIGKDD International Conference on Knowledge Discovery and Data Mining*, 2016, pp. 785–794. [Online]. Available: <http://doi.acm.org/10.1145/2939672.2939785>
- [28] Anas Z. Abidin, Adorma M. DSouza, Axel Wismuller, "Detecting connectivity changes in autism spectrum disorder using large-scale Granger causality," *SPIE*, Proceedings, no. 10949, 2109.
- [29] H. Zou and L. Xue, "A Selective Overview of Sparse Principal Component Analysis," *Proc. IEEE*, vol. 106, no. 8, pp. 1311–1320, 2018, doi: 10.1109/JPROC.2018.2846588.
- [30] F.-C. Yeh *et al.*, "Population-averaged atlas of the macroscale human structural connectome and its network topology," *NeuroImage*, vol. 178, pp. 57–68, 2018, doi: 10.1016/j.neuroimage.2018.05.027.
- [31] P. S. Dhillon, D. A. Wolk, S. R. Das, L. H. Ungar, J. C. Gee, and B. B. Avants, "Subject-specific functional parcellation via prior based eigenanatomy," *NeuroImage*, vol. 99, pp. 14–27, 2014, doi: 10.1016/j.neuroimage.2014.05.026.
- [32] A. Schaefer *et al.*, "Local-Global Parcellation of the Human Cerebral Cortex from Intrinsic Functional Connectivity MRI," *Cerebral cortex (New York, N.Y. : 1991)*, vol. 28, no. 9, pp. 3095–3114, 2018, doi: 10.1093/cercor/bhx179.
- [33] E. T. Rolls, C.-C. Huang, C.-P. Lin, J. Feng, and M. Joliot, "Automated anatomical labelling atlas 3," *NeuroImage*, vol. 206, p. 116189, 2020, doi: 10.1016/j.neuroimage.2019.116189.
- [34] D. C. van Essen *et al.*, "The Human Connectome Project: A data acquisition perspective," *NeuroImage*, vol. 62, no. 4, pp. 2222–2231, 2012, doi: 10.1016/j.neuroimage.2012.02.018.
- [35] T. D. Satterthwaite, R. Ciric, D. R. Roalf, C. Davatzikos, D. S. Bassett, and D. H. Wolf, "Motion artifact in studies of functional connectivity: Characteristics and mitigation strategies," *Hum. Brain Mapp.*, vol. 40, no. 7, pp. 2033–2051, 2019, doi: 10.1002/hbm.23665.
- [36] M. F. Glasser *et al.*, "The minimal preprocessing pipelines for the Human Connectome Project," *NeuroImage*, vol. 80, pp. 105–124, 2013, doi: 10.1016/j.neuroimage.2013.04.127.
- [37] C. J. Stoodley, E. M. Valera, and J. D. Schmahmann, "Functional topography of the cerebellum for motor and cognitive tasks: An fMRI study," *NeuroImage*, vol. 59, no. 2, pp. 1560–1570, 2012, doi: 10.1016/j.neuroimage.2011.08.065.
- [38] J. C. Bezdek and N. R. Pal, "Some new indexes of cluster validity," *IEEE transactions on systems, man, and cybernetics. Part B, Cybernetics : a publication of the IEEE Systems, Man, and Cybernetics Society*, vol. 28, no. 3, pp. 301–315, 1998, doi: 10.1109/3477.678624.
- [39] E. S. Finn *et al.*, "Functional connectome fingerprinting: Identifying individuals using patterns of brain connectivity," *Nature neuroscience*, vol. 18, no. 11, pp. 1664–1671, 2015, doi: 10.1038/nn.4135.
- [40] W. Wu *et al.*, "An electroencephalographic signature predicts antidepressant response in major depression," *Nature Biotechnology*, vol. 38, no. 4, pp. 439–447, 2020, doi: 10.1038/s41587-019-0397-3.
- [41] L. Geerligs, K. A. Tsvetanov, Cam-Can, and R. N. Henson, "Challenges in measuring individual differences in functional connectivity using fMRI: The case of healthy aging," *Human brain mapping*, vol. 38, no. 8, pp. 4125–4156, 2017, doi: 10.1002/hbm.23653.
- [42] M. Pannunzi *et al.*, "Resting-state fMRI correlations: From link-wise unreliability to whole brain stability," *NeuroImage*, vol. 157, pp. 250–262, 2017, doi: 10.1016/j.neuroimage.2017.06.006.
- [43] C. C. Guo *et al.*, "One-year test-retest reliability of intrinsic connectivity network fMRI in older adults," *NeuroImage*, vol. 61, no. 4, pp. 1471–1483, 2012, doi: 10.1016/j.neuroimage.2012.03.027.
- [44] J. Wang *et al.*, "Test-retest reliability of functional connectivity networks during naturalistic fMRI paradigms," *Human brain mapping*, vol. 38, no. 4, pp. 2226–2241, 2017, doi: 10.1002/hbm.23517.
- [45] X.-H. Liao *et al.*, "Functional brain hubs and their test-retest reliability: a multiband resting-state functional MRI study," *NeuroImage*, vol. 83, pp. 969–982, 2013, doi: 10.1016/j.neuroimage.2013.07.058.

8 Supplement

8.1.1 Connectivity matrix organization

Figure 2 and **Figure 3** display average connectivity matrices organized according to the diagram in **Supplementary Figure S1**. This figure shows how the rows and columns are organized anatomically by hemisphere and by resting state network (RSN). The cortical regions are sorted first by left/right hemisphere and then by RSN, while the subcortical and cerebellar regions are sorted first by subcortical region and then by left/right hemisphere.



8.1.2 Effective connectivity stability

To further differentiate between the different causal connectivity metrics, we quantified the stability of these measures as a function of the portion of the timeseries considered. An ideal metric would be highly reproducible even if calculated on a small fraction of the timeseries. **Supplementary Figure S2** shows the performances of some of the top EC measures that performed similarly, namely $\text{Elastic}_{\lambda=0.01}\text{GC}$, PCAGC , and $\text{SPGC}_{\text{fine}}$. MLEC_{ERT} was left out of this analysis due to its low performance in Experiment 2. The reliability of $\text{SPGC}_{\text{fine}}$ is significantly higher than the other methods, and maintains this higher reproducibility across

all lengths of time analyzed. Notably, $SPGC_{fine}$ using 50% of the initial timeseries has a higher reproducibility than the Elastic GC or PCAGC methods using 100% of the timeseries. This stability with less of the timeseries used is also desirable.

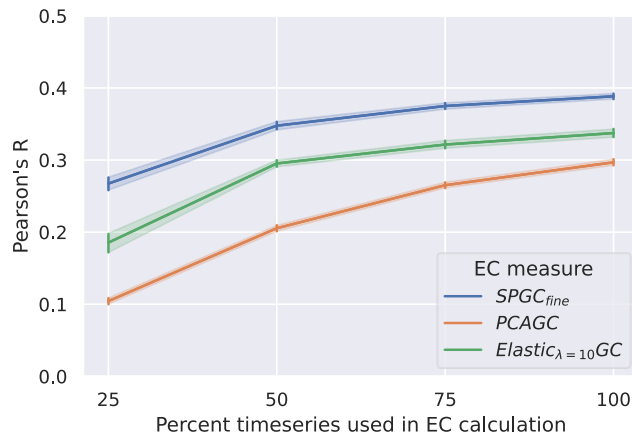


Figure S2: Reliability of effective connectivity using a partial timeseries. The reproducibility as measured by Pearson's r for every pair of EC matrices in the four scan set per subject is shown versus the percent of the initial timeseries used. 25% of the timeseries used indicates that the first 25% of the original timeseries was used to calculate EC and then the reliability was calculated amongst that set that used only 25% of the original timeseries. The 95% CI is shown with error bars and shaded area.